AGU PUBLICATIONS

JGR

Journal of Geophysical Research: Atmospheres

RESEARCH ARTICLE
10.1002/2016JD026303

**Key Points:**
- Tropical mean high cloud fractions decrease with increasing surface temperature ($T_s$) at a rate of about $-1\%\ K^{-1}$ from 2002 to 2015
- Cirrostratus and deep convective clouds contribute primarily to the decrease of tropical mean high cloud fraction with surface warming
- High cloud fraction response accounts for ~16% of the interannual tropical mean precipitation increase per unit surface warming

**Correspondence to:**
R. Liu,
liuruncn@163.com

**Citation:**
Liu, R., K.-N. Liou, H. Su, Y. Gu, B. Zhao, J. H. Jiang, and S. C. Liu (2017), High cloud variations with surface temperature from 2002 to 2015: Contributions to atmospheric radiative cooling rate and precipitation changes, *J. Geophys. Res. Atmos.*, *122*, 5457–5471, doi:10.1002/2016JD026303.

Received 28 NOV 2016
Accepted 9 MAY 2017
Accepted article online 11 MAY 2017
Published online 27 MAY 2017



# High cloud variations with surface temperature from 2002 to 2015: Contributions to atmospheric radiative cooling rate and precipitation changes

**Run Liu[1], Kuo-Nan Liou[1,2], Hui Su[3], Yu Gu[1,2], Bin Zhao[1], Jonathan H. Jiang[3], and Shaw Chen Liu[4]**

[1]Joint Institute for Regional Earth System Science and Engineering, University of California, Los Angeles, California, USA, [2]Department of Atmospheric and Oceanic Sciences, University of California, Los Angeles, California, USA, [3]Jet Propulsion Laboratory, California Institute of Technology, Pasadena, California, USA, [4]Environmental and Climate Institute, Jinan University, Guangzhou, China

**Abstract** The global mean precipitation is largely constrained by atmospheric radiative cooling rates ($Q_r$), which are sensitive to changes in high cloud fraction. We investigate variations of high cloud fraction with surface temperature ($T_s$) from July 2002 to June 2015 and compute their radiative effects on $Q_r$ using the Fu-Liou-Gu plane-parallel radiation model. We find that the tropical mean (30°S–30°N) high cloud fraction decreases with increasing $T_s$ at a rate of about $-1.0 \pm 0.34\%\ K^{-1}$ from 2002 to 2015, which leads to an enhanced atmospheric cooling around $0.86\ W\ m^{-2}\ K^{-1}$. On the other hand, the northern midlatitudes (30°N–60°N) high cloud fraction increases with surface warming at a rate of $1.85 \pm 0.65\%\ K^{-1}$ and the near-global mean (60°S–60°N) high cloud fraction shows a statistically insignificant decreasing trend with increasing $T_s$ over the analysis period. Dividing high clouds into cirrus, cirrostratus, and deep convective clouds, we find that cirrus cloud fraction increases with surface warming at a rate of $0.32 \pm 0.11\%\ K^{-1}$ ($0.01 \pm 0.17\%\ K^{-1}$) for the near-global mean (tropical mean), while cirrostratus and deep convective clouds decrease with surface warming at a rate of $-0.02 \pm 0.18\%\ K^{-1}$ and $-0.33 \pm 0.18\%\ K^{-1}$ for the near-global mean and $-0.64 \pm 0.23\%\ K^{-1}$ and $-0.37 \pm 0.13\%\ K^{-1}$ for the tropical mean, respectively. High cloud fraction response to feedback to $T_s$ accounts for approximately $1.9 \pm 0.7\%$ and $16.0 \pm 6.1\%$ of the increase in precipitation per unit surface warming over the period of 2002–2015 for the near-global mean and the tropical mean, respectively.

## 1. Introduction

Precipitation is of great importance to the welfare of human beings as well as the entire ecosystem [*Trenberth*, 2011]. The increase in global mean precipitation per unit surface warming is a measure of hydrological cycle intensification, serving as a first-order constraint on regional precipitation change [*Pendergrass and Hartmann*, 2014a]. In a warmer climate, the saturation water vapor increases with atmospheric temperature approximately following the Clausius-Clapeyron relation at a rate of about $7\%\ K^{-1}$, while the global mean precipitation is governed by atmospheric energy budget [*Mitchell et al.*, 1987; *Allen and Ingram*, 2002] and increases at a rate of $1–3\%\ K^{-1}$ [*Allen and Ingram*, 2002]. Since the atmospheric heat storage is small on annual and longer timescales [*Lambert et al.*, 2015], the global mean net atmospheric radiative cooling ($Q_r$, positive sign for atmospheric cooling) is balanced by the sensible heating (SH) from the surface and latent heat release associated with precipitation rate multiplied by the latent heat of vaporization ($L_vP$). The atmospheric energy balance may be written as follows:

$$Q_r = L_vP + \mathrm{SH} \tag{1}$$

Thus, the energy constraint on precipitation suggests that changes in global mean precipitation would depend on the changes in $Q_r$ and SH. The magnitude of $Q_r$ dominates over that of SH. Also, the change in SH contributes to this balance but is much smaller in magnitude [e.g., *Lambert and Webb*, 2008; *Wild et al.*, 2013; *Pendergrass and Hartmann*, 2014b]; therefore, this study focuses on the changes in $Q_r$ and their contribution to precipitation changes from 2002 to 2015, during which abundant satellite observations are available.

Globally, clouds cover roughly two thirds of Earth's surface and are important to modulate Earth's energy budget [e.g., *Arking*, 1991; *Mace et al*., 2009]. Cloud radiative effects (CREs) can alter $Q_r$ and thus affect precipitation. The CREs on $Q_r$ depend on cloud vertical height and optical depth. In general, low clouds tend to have a net cooling effect by increasing the downward emission of longwave (LW) radiation and reflecting solar radiation, while high clouds tend to warm the atmosphere by decreasing the upward emission of LW radiation [e.g., *Slingo and Slingo*, 1988; *Hartmann and Larson*, 2002; *Kuang and Hartmann*, 2007]. In general, high clouds play a relatively stronger role than low clouds in altering $Q_r$. For instance, *Pendergrass and Hartmann* [2014b] showed that a single-layered low cloud in the boundary layer with a liquid water path of 40 g $m^{-2}$ would increase $Q_r$ by about 29 W $m^{-2}$, while high clouds of the same optical depth but situated between 5.5 and 12 km would reduce net $Q_r$ by about 103 W $m^{-2}$, about 3.6 times of the effect exerted by the low clouds of the same liquid water path.

It has been hypothesized that the tropical high cloud fraction would decrease in response to surface warming [*Lindzen et al*., 2001]. The so-called "iris hypothesis" stated that an increased sea surface temperature would enhance convective precipitation but reduce cirrus detrainment, resulting in a shrinkage of high cloud cover, i.e., an expansion of dry and clear regions of the tropical atmosphere. This would allow more infrared radiation leakage from the Earth's atmosphere, which constitutes a negative feedback on surface warming. There have been intense debates about the validity of the iris hypothesis and its implications [e.g., *Hartmann and Michelsen*, 2002; *Lin et al*., 2002, 2004; *Spencer et al*., 2007; *Su et al*., 2008, 2010a, 2010b; *Lindzen and Choi*, 2011; *Mauritsen and Stevens*, 2015]. *Mauritsen and Stevens* [2015] showed that amplifying the "iris effect" in ECHAM6 (European Centre/Hamburg) model would reduce the discrepancies between the simulated and observed rates of outgoing longwave radiation increases with surface temperature ($T_s$). The ECHAM6 model sensitivity experiments suggested that a greater decrease in high cloud fraction with surface warming would produce a higher hydrological sensitivity because the increased LW radiative cooling of the atmosphere associated with reduced high clouds must be balanced by enhanced latent heat release. It is not clear whether observations show a detectable decrease in high cloud fraction with surface warming and how much it would contribute to the observed precipitation sensitivity through its effect on atmospheric cooling rate.

In view of the above, this study focuses on variations of high clouds and associated radiative effects on $Q_r$ during the A-Train period when high-quality satellite observations of clouds have become available [*L'Ecuyer and Jiang*, 2010]. Concurrent observations of global mean precipitation variations are analyzed, and the contribution of high cloud radiative effects to precipitation changes is quantified. We note that our analysis focuses on the interannual variabilities and whether the interannual relations are applicable to long-term climate change requires further studies.

In addition, it is known that high clouds of different optical depths would produce distinct sensitivities to surface warming. For example, it was found that the cirrus cloud fraction increases in response to surface warming [*Zhou et al*., 2014], while deep convective clouds and associated anvils exhibit a decreasing trend with increasing $T_s$ [*Zelinka and Hartmann*, 2011]. Net high cloud effects are therefore the residual of those competing effects, resulting in large uncertainties. It is critically important to distinguish the impacts of different types of high clouds in order to have better understanding of cloud feedbacks. Different from the aforementioned studies, we focus on high cloud effects on atmospheric column cooling rate, instead of CREs on the top of atmosphere (TOA), because the former is directly related to the global mean or tropical mean precipitation change constrained by atmospheric energy balance.

To quantify the radiative effects of high clouds, we use the Fu-Liou-Gu (FLG) plane-parallel radiative transfer model [*Fu and Liou*, 1992, 1993; *Gu et al*., 2003, 2006, 2010] to calculate $Q_r$ associated with different types of high clouds. In section 2, we describe the data and FLG model used. In section 3, we first validate FLG model calculations by comparison with CERES-EBAF (Clouds and the Earth's Radiant Energy System Energy Balance and Filled) products [*Wielicki et al*., 1996; *Loeb et al*., 2009; *Kato et al*., 2013]. We then examine variations of the high cloud fraction (including three subtypes) in response to $T_s$ during the A-Train period and compute the sensitivity of high cloud effects on $Q_r$ per unit surface warming. This is followed by estimating the contribution of high cloud fraction change to precipitation sensitivity. Lastly, conclusions are given in section 4.

## 2. The FLG Radiative Transfer Model and Data Used

The FLG plane-parallel radiation model [*Fu and Liou*, 1992, 1993; *Gu et al*., 2003, 2006, 2011] uses the delta-four-stream approximation for shortwave (SW) and LW flux calculations [*Liou et al*., 1988; *Fu et al*., 1997]. The solar (0–5 μm) and infrared (5–50 μm) spectra are divided into 6 and 12 bands, respectively, within which the correlated *k*-distribution method developed by *Fu and Liou* [1992] is used to sort gaseous absorption lines. FLG model has been extensively used [e.g., *Zhang et al*., 2013; *Campbell et al*., 2016; *Zhao et al*., 2016] and is incorporated in the Weather Research Forecast as a new radiation module [*Gu et al*., 2010].

In this study, the vertical layer setting in the FLG model follows the ERA-Interim vertical dimension, which is defined by an eta coordinate whereby a purely pressure coordinate at the top and upper levels of the model atmosphere transitions to a hybrid pressure-sigma coordinate at middle to low level and finally to a terrain-following sigma corrdinate at the lowest few levels and model surface. The 10 vertical levels chosen from TOA to surface are levels of 22, 28, 35, 36, 49, 44, 48, 53, and 60 (ranging from 50 hPa to 1000 hPa). The pressure at level *j* can be calculated according to *European Centre for Medium-Range Weather Forecasts* (*ECMWF*) [2002] as follows:

$$p_j = a_j + b_j P_s \tag{2}$$

where $P_s$ is surface pressure. Time-independent coefficients $a_j$ and $b_j$ can be obtaind from *ECMWF* [2002].

We use the Moderate Resolution Imaging Spectroradiometer (MODIS) Level 3 Collection 6 monthly cloud products from Aqua [*King et al*., 2003] (http://daac.gsfc.nasa.gov/MODIS/products.shtml), available at a 1° × 1° resolution, covering the period from July 2002 to June 2015 to conduct the investigation. The MODIS cloud products provide cloud fraction ($C$(lon,lat,$P_{\mathrm{top}}$,$\tau$,mon)) for seven optical depth bins and seven vertical layers. Following the definitions of cloud types by the International Satellite Cloud Climatology Project [*Rossow and Schiffer*, 1999], high clouds (with cloud top pressure less than 440 hPa) are further categorized by their optical depth ($\tau$) into cirrus ($\tau \le 3.6$), cirrostratus ($3.6 < \tau \le 23$), and deep convective ($\tau > 23$) clouds. It should be noted that this cloud classification differs from that given by the World Meteorological Organization, which sorts high clouds into cirrus, cirrocumulus, and cirrostratus [*World Meteorological Organization*, 1975].

The MODIS cloud products also provide the integrated optical depth within the atmosphere. The optical depth for each individual level cloud is needed for FLG model calculations and is weighted by cloud fraction denoted by $C$(lon,lat,$P_{\mathrm{top}}$,$\tau$,mon) according to the following equation:

$$\tau(\mathrm{lon},\mathrm{lat},P_{\mathrm{top}},\mathrm{mon}) = \sum_{i=1}^{7}\left(C(\mathrm{lon},\mathrm{lat},P_{\mathrm{top}},\tau_i,\mathrm{mon})\times\tau_i\right)/\sum_{i=1}^{7}C(\mathrm{lon},\mathrm{lat},P_{\mathrm{top}},\tau_i,\mathrm{mon}) \tag{3}$$

where $\tau_i$ = 0.15, 0.8, 2.45, 6.5, 16.2, 41.5, and 80 representing the middle value for each optical depth bin.

We use maximum/random cloud overlapping schemes for all-sky condition radiative fluxes calculation; i.e., maximum overlapping assumption is used within the broad layers for low, middle, and high clouds separately and random overlapping assumption is used for the overlapping between the low, middle, and high clouds [*Gu et al*., 2003]. Radiation calculation is performed for each scenario of layered clouds, and then the all-sky flux is determined as the sum of the fluxes computed for each scenario weighted by cloud amounts.

The liquid cloud water content (LWC) and ice cloud water content (IWC) are then calculated from the optical depth based on the empirical function. According to the analysis presented in equation (2.9) in *Fu and Liou* [1993], IWC (in units of g $\mathrm{m}^{-3}$) is given by

$$\mathrm{IWC} = \tau\sum_{1}^{3} a_n D_e^n/\mathrm{d}Z \tag{4}$$

where d$Z$ is the distance (in units of m) between any two vertical levels and $D_e$ (in units of μm) is the effective size of ice particles. For global calculations, $D_e$ is set at 80 μm [*Gu et al*., 2006]. The fitting coefficients $a_1$, $a_2$, and $a_3$ are 0.2453, $1.2196\times10^{-3}$, and $-3.4745\times10^{-6}$, respectively.

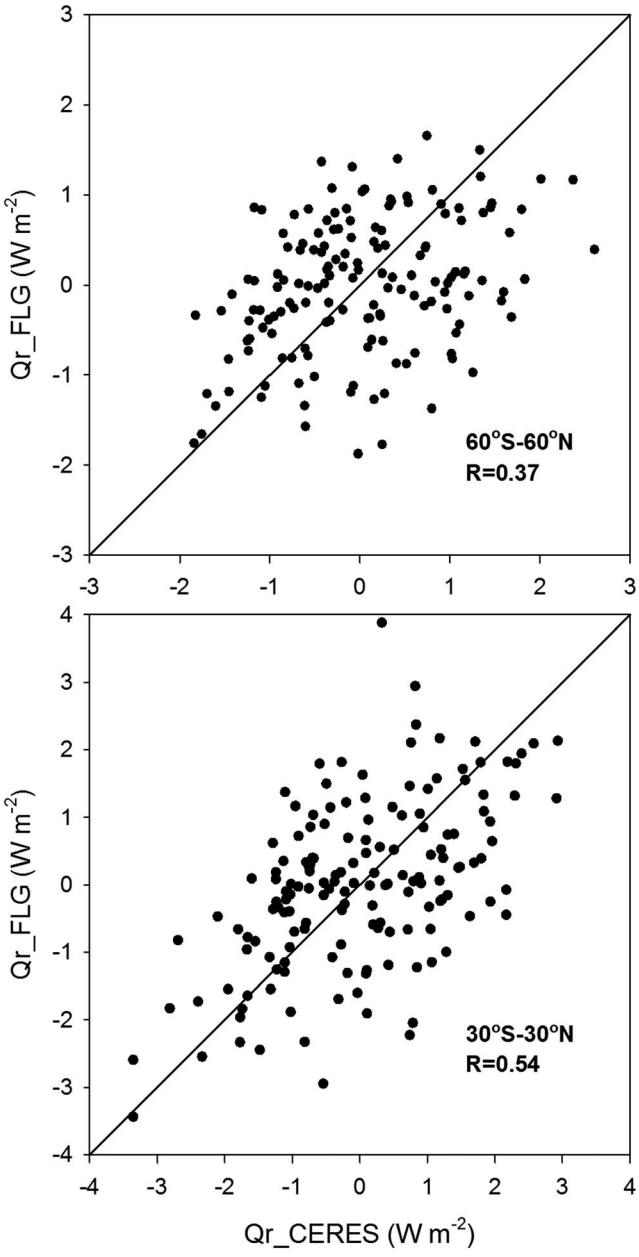


**Figure 1.** Scatterplots of the deseasonalized monthly $Q_r$ derived from the FLG model ($Q_{r\_FLG}$) against $Q_r$ analyzed from CERES-EBAF observations ($Q_{r\_CERES}$) under all-sky conditions for (top) the near-global region and (bottom) the tropics. The correlation coefficients are also shown in the figure.

For liquid water clouds, the following formula is employed to calculate LWC (in units of g $m^{-3}$) in the form [*Fu and Liou*, 1993]

$$\mathrm{LWC} = \frac{4}{3} R_e \tau / \sum_1^3 b_n (\ln R_e)^{n-1} / \mathrm{d}Z \tag{5}$$

where $R_e$ is the effective radius of water droplets (10 μm) [see *Gu et al*., 2003]. The fitting coefficients $b_1$, $b_2$, and $b_3$ are 2.416, −0.1854, and 0.0209, respectively.

These values of $R_e$ and $D_e$ are based on our best knowledge of liquid and ice clouds in global and tropical conditions as well as the closet match between model-simulated and observed radiative fluxes. The sensitivity of the calculated $Q_r$ to the cloud particle size assumption is discussed.

Meteorological variables in terms of temperature, pressure, humidity, surface albedo, and ozone concentrations required in the FLG model are obtained from ERA-Interim reanalysis [*Dee et al*., 2011]. To validate FLG model calculations, we use observed radiative fluxes taken from CERES-EBAF products (https://ceres.larc.nasa.gov/order_data.php) [*Wielicki et al*., 1996; *Loeb et al*., 2009; *Kato et al*., 2013]. Precipitation data employed in this study are taken from the Global Precipitation Climatology Project (GPCP) Monthly version 2.2 [*Adler et al*., 2003]. $T_s$ is obtained from the HadCRUT4 data set [*Morice et al*., 2012].

The near-global domain covering 60°S–60°N is analyzed along with three subregions, which include the tropics (30°S–30°N), the northern midlatitudes (30°N–60°N), and the southern midlatitudes (30°S–60°S). We define deseasonalized anomalies $\Delta X$ as follows:

$$\Delta X = X - \overline{X} \tag{6}$$

where $X$ is a parameter, which can be $T_s$, $L_vP$, cloud fraction, or radiative flux, for a given month and $\overline{X}$ denotes the monthly climatological mean. For instance, for $n$ years of data, the climatological mean computed from each January value is used to obtain the deseasonalized anomaly. We then regress the deseasonalized $L_vP$,

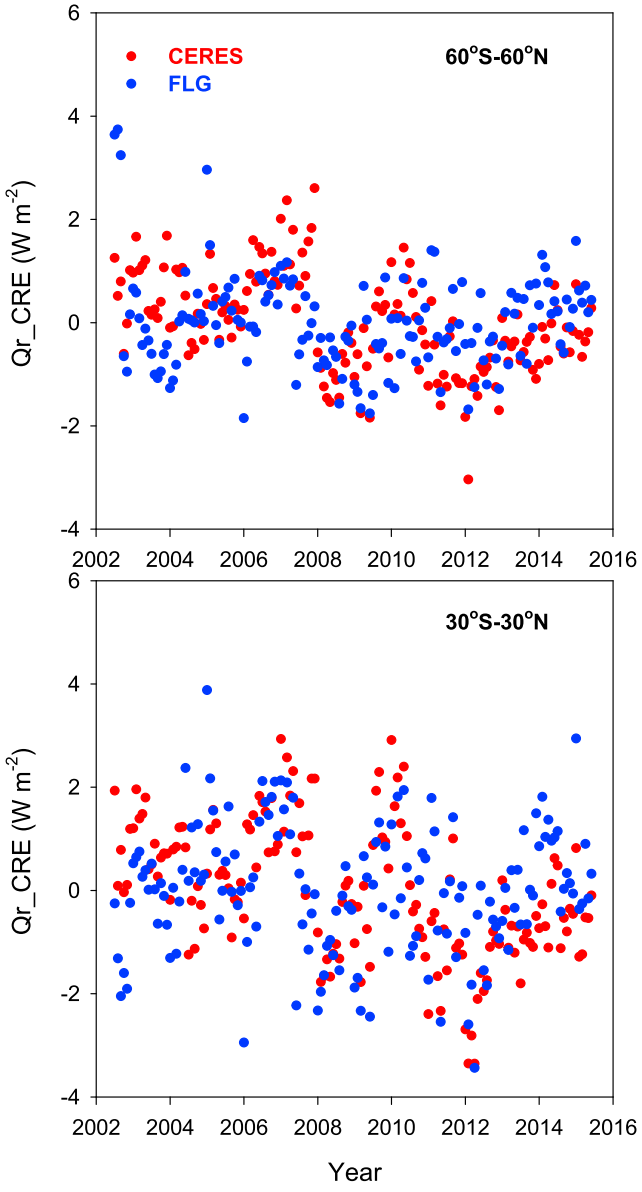


**Figure 2.** Time series of the deseasonalized monthly $Q_r$ derived from the FLG model (blue) and $Q_r$ analyzed from CERES-EBAF observations (red) under all-sky conditions for (top) the near-global mean and (bottom) the tropical mean.

cloud fraction, or radiative flux data to the deseasonalized $T_s$ associated with a monthly timescale by the ordinary least squares regression such that the regression slope represents their sensitivity to changes in $T_s$.

In this study, $Q_r$ is calculated as follows:

$$Q_r = F_{\mathrm{uir\_TOA}} + F_{\mathrm{us\_TOA}} - F_{\mathrm{ds\_TOA}} + F_{\mathrm{dir\_SFC}} - F_{\mathrm{uir\_SFC}} + F_{\mathrm{ds\_SFC}} - F_{\mathrm{us\_SFC}} \quad (7)$$

All fluxes are defined positive at a given direction. Subscripts u, d, ir, s, TOA, and SFC denote upward, downward, LW, SW, the top of atmosphere, and the surface, respectively. Positive values of $Q_r$ represent radiative cooling rates in the atmospheric column. The analysis period is from July 2002 to June 2015, during which all relevant data sets are available.

## 3. Results and Discussions

### 3.1. Comparison Between Radiative Fluxes Calculated From the FLG Model and the CERES-EBAF Products

Figure 1 compares the deseasonalized monthly $Q_r$ derived from the FLG model ($Q_{r\_\mathrm{FLG}}$) with CERES-EBAF products ($Q_{r\_\mathrm{CERES}}$) under all-sky conditions for averages over the near-global region (top) and the tropics (bottom). The correlation coefficients between $Q_{r\_\mathrm{FLG}}$ and $Q_{r\_\mathrm{CERES}}$ ($R$ = 0.37 and 0.54 for near-global and tropics, respectively) show that FLG model calculations approximately capture 14%–30% variance in $Q_r$ observed by CERES. In addition, the temporal evolutions in monthly $Q_r$ under all-sky conditions from CERES and FLG calculations agree with each other, as shown in Figure 2. The spatial distributions of multiyear means from CERES and FLG calculations are also similar (Figure 3), with spatial correlations of 0.90 and 0.92, for all-sky conditions (Figures 3a and 3b) and CRE (Figures 3c and 3d), respectively. However, there is an underestimation in $Q_{r\_\mathrm{FLG}}$ compared to $Q_{r\_\mathrm{CERES}}$, which is mainly related to LW radiative flux components (Figure 4) due to the cold bias in $T_s$ [e.g., *Jones and Harpham*, 2013; *Wang et al.*, 2015] as well as the wet bias in specific humidity [e.g., *Kishore et al.*, 2011; *Schröder et al.*, 2013; *Jiang et al.*, 2015] in ERA-Interim reanalysis leading to a reduced LW emission at the surface and enhanced LW absorption within the atmosphere. A prescribed cloud particle size is also a potential source for the difference between $Q_{r\_\mathrm{FLG}}$ and $Q_{r\_\mathrm{CERES}}$. Varying the cloud particle size results in differences in the magnitude of $Q_r$ by

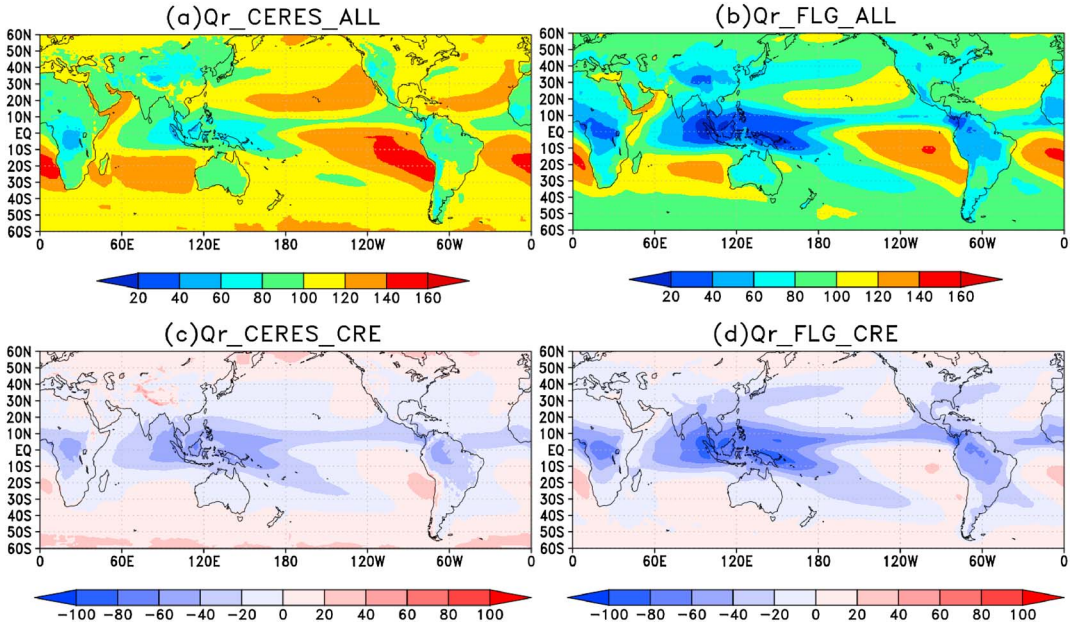


**Figure 3.** Multiyear mean (July 2002 to June 2015) $Q_r$ under (a and b) all-sky conditions and (c and d) total CRE. Figures 3a and 3c are CERES-EBAF products, and Figures 3b and 3d are calculated from the FLG model. Positive/negative values in Figures 3c and 3d indicate a cooling/warming effect within the atmosphere.

7%. Nevertheless, the temporal variations of $Q_r$, which are the main focus of this study, are consistent when different cloud particle sizes are used (Figure 5). Uncertainty from CERES data is also a source of the inconsistency.

The CRE calculated from FLG resembles that derived from CERES-EBAF in terms of spatial patterns (Figures 3c and 3d) with an overestimate over the western Pacific region. Despite the biases in calculated $Q_r$ magnitudes,

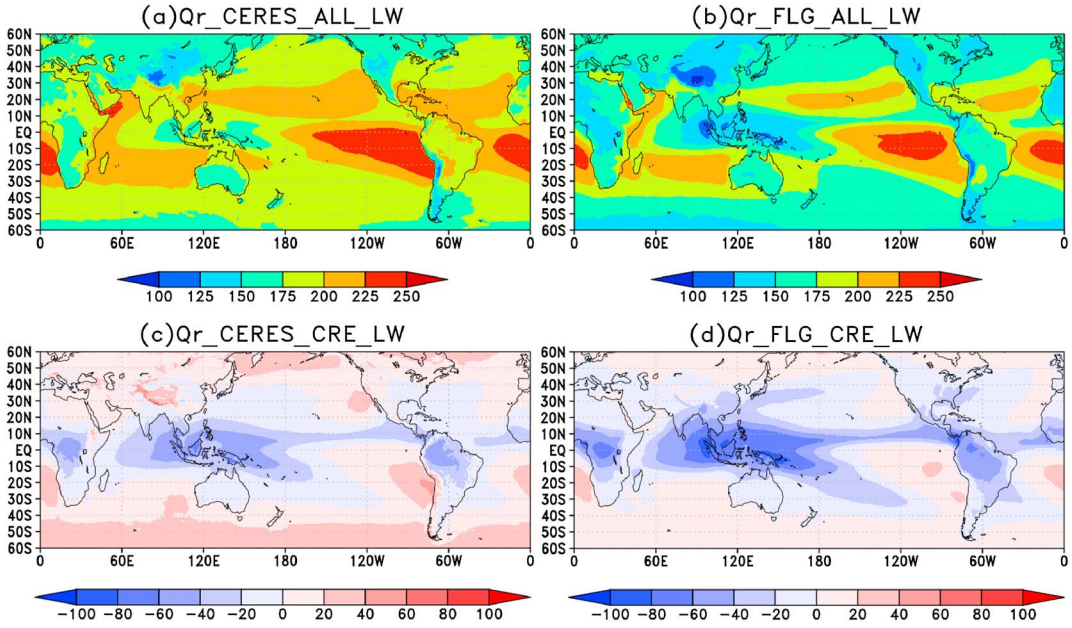


**Figure 4.** Multiyear mean (July 2002 to June 2015) $Q_r$ LW radiative components under (a and b) all-sky conditions and in (c and d) total CRE. Figures 4a and 4c are CERES-EBAF products, while Figures 4b and 4d are calculated from the FLG model.

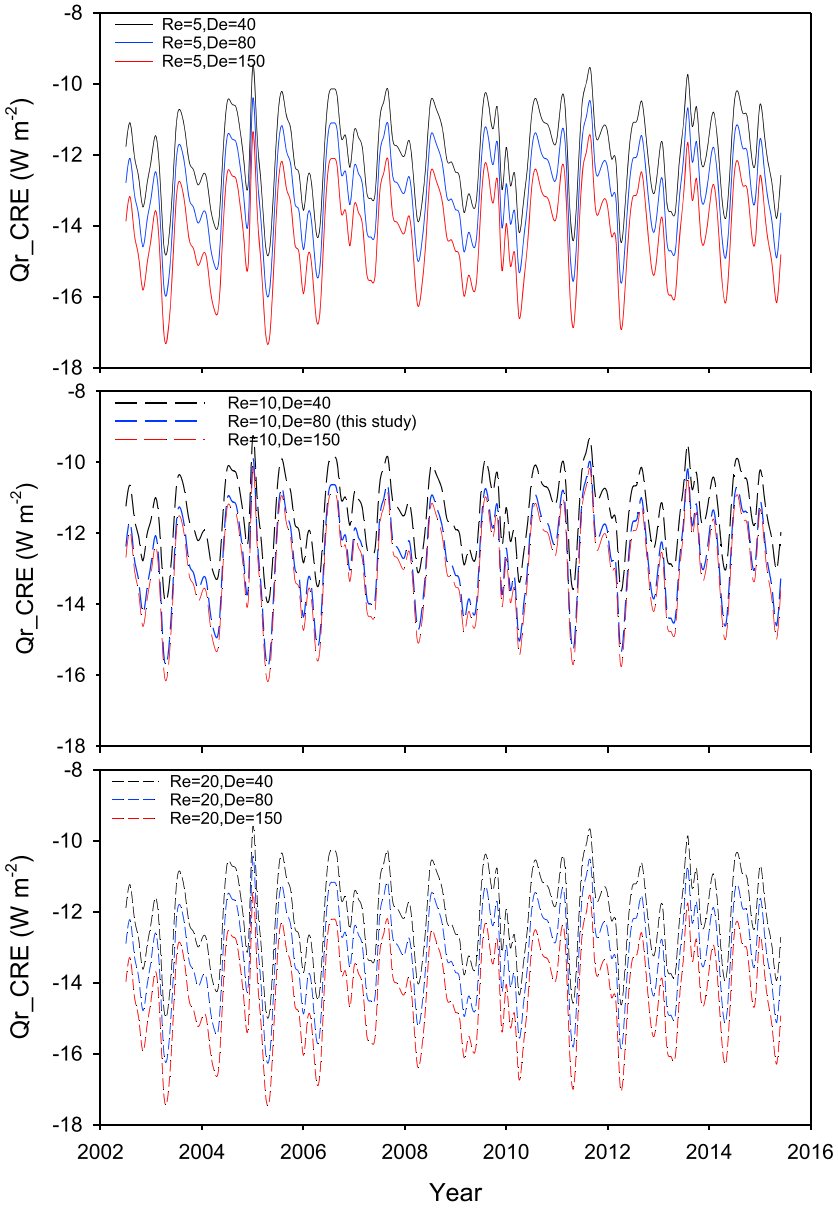


**Figure 5.** Time series of monthly total cloud effect on $Q_r$ for the near-global mean with varying cloud particle sizes. Black, blue, and red are for $D_e$ of 40 μm, 80 μm, and 150 μm, respectively. Solid, long-dash, and short-dash lines are for $R_e$ of (top) 5 μm, (middle) 10 μm, and (bottom) 20 μm, respectively.

the FLG model captures the temporal evolution of observed radiative fluxes during the period of 2002–2015, which is the focus of this study.

### 3.2. High Cloud Impact on Atmospheric Radiative Cooling

The high cloud effects on $Q_r$ are defined by the difference between the $Q_r$ calculated with and without high clouds present, while all other (surface and atmospheric) quantities remain unchanged. The positive cloud effects on $Q_r$ indicate that high cloud changes induce an increase in the cooling rate within the atmosphere, and vice versa. Figures 6 and 7 depict the total and three subtypes of high cloud effects on $Q_r$ and associated contributions from LW and SW radiative flux components. Most high clouds occur near the equator and over tropical continents [e.g., *Wylie and Menzel*, 1999; *Stubenrauch et al.*, 2010, 2013], and some are present over midlatitudes storm track regions. The frequent occurrence of high clouds in the tropics accounts for larger CREs than in other regions. In general, when high clouds are present, the loss of LW radiation to space

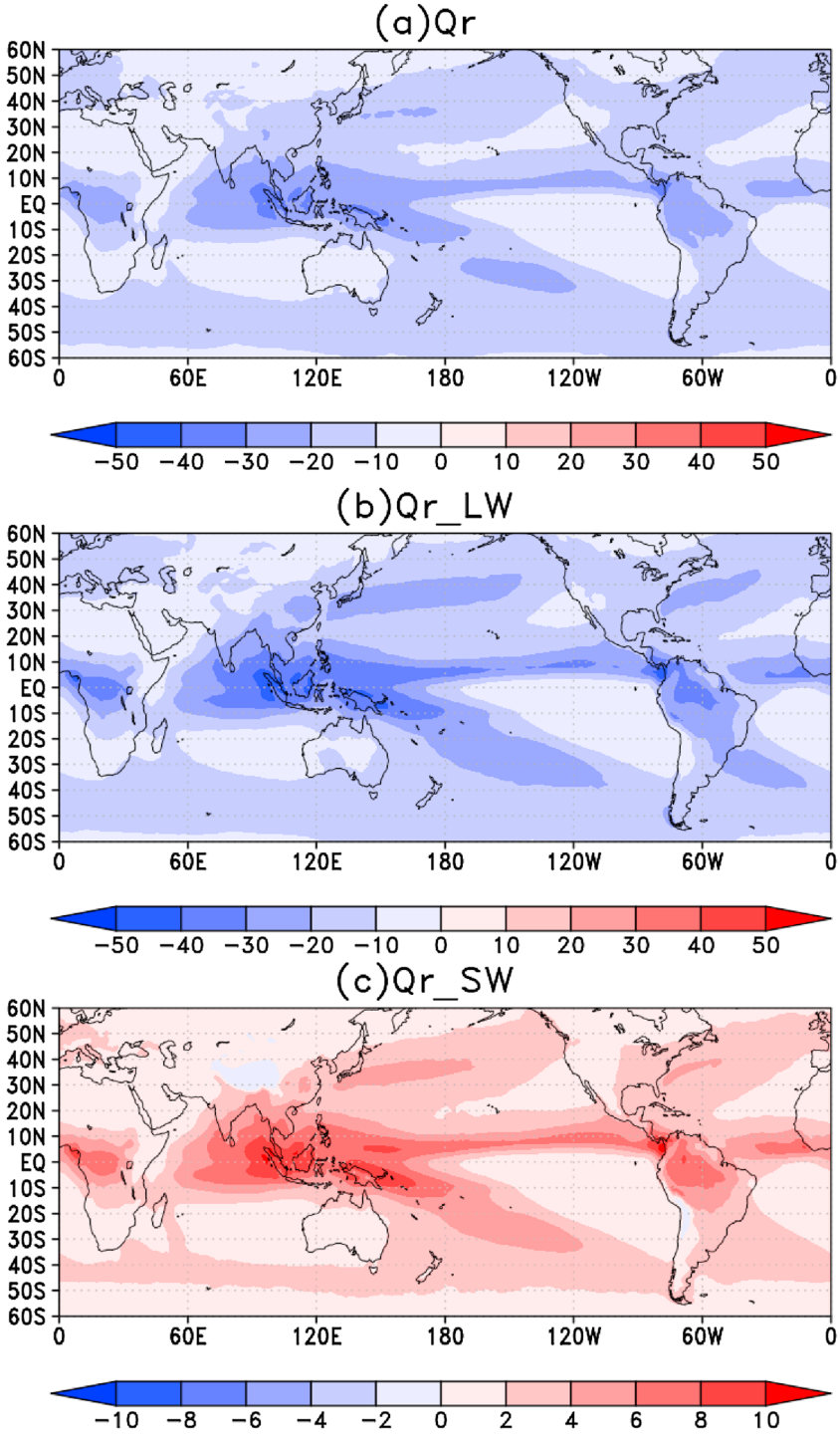


**Figure 6.** (a) High cloud effects on $Q_r$ and contributions of (b) LW components and (c) SW components during July 2002 to June 2015 (in units of W $m^{-2}$). The positive (negative) values indicate that high clouds have a positive (negative) effect on $Q_r$, corresponding to a cooling (warming) effect within the atmosphere.

decreases, resulting in a warming effect in the atmosphere, whereas the reflection of SW radiation also increases and leads to a cooling effect. For the atmospheric column, the LW warming effect predominates over the SW cooling effect, resulting in a decrease in atmosphere cooling, i.e., a negative impact on $Q_r$ (Figure 6a). The finding that high clouds reduce atmospheric radiative cooling because of their LW

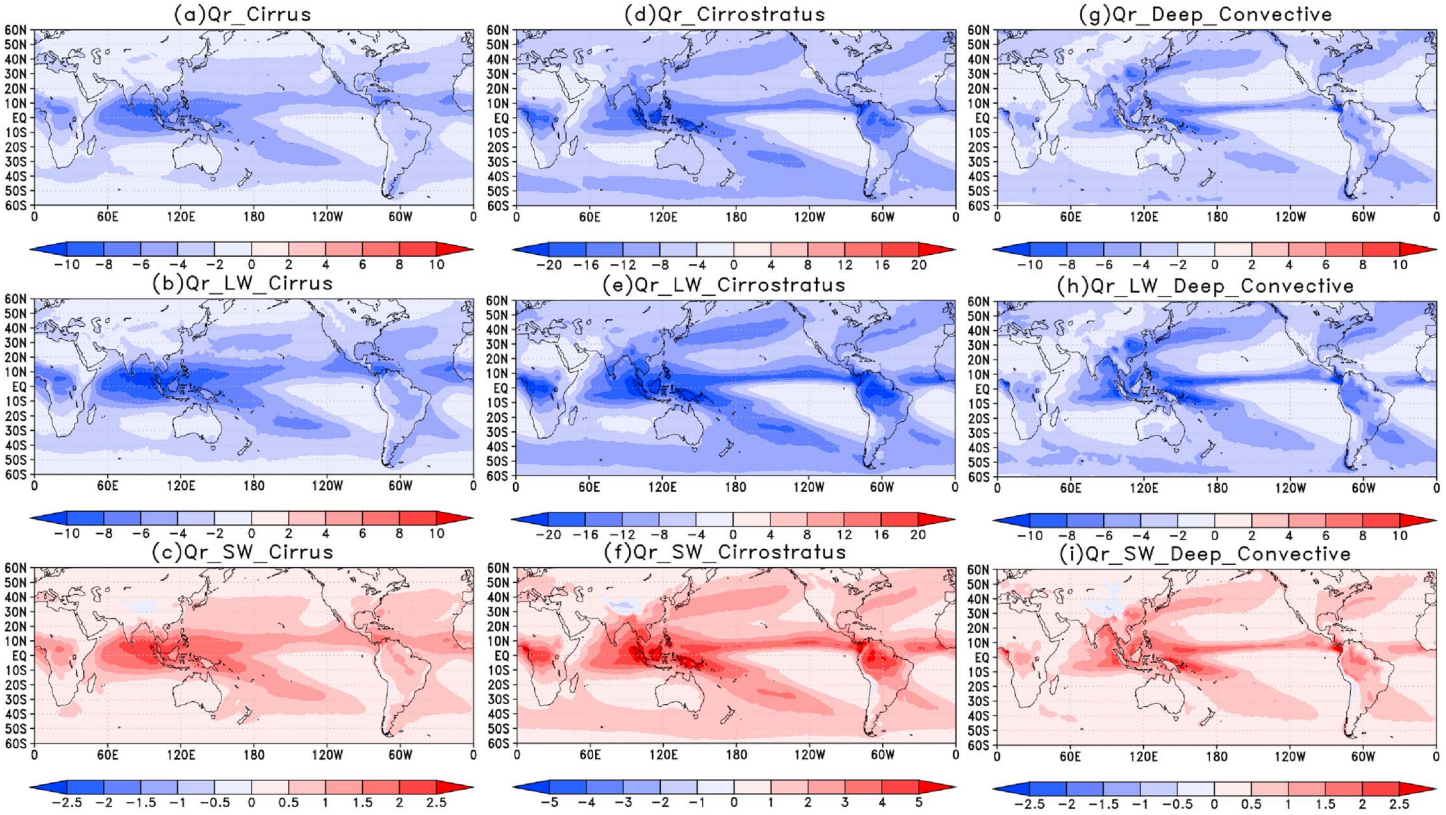


**Figure 7.** Same as Figure 6 except for (a–c) cirrus ($\tau \leq 3.6$), (d–f) cirrostratus ($3.6 < \tau \leq 23$), and (g–i) deep convective cloud ($\tau > 23$).

effects, which are compensated only slightly by SW effects, is consistent with previous findings reported by *Pendergrass and Hartmann* [2014b] because atmospheric absorption of SW radiation is relatively small compared to that of LW radiation.

The three subtypes of high clouds, cirrus, cirrostratus, and deep convective clouds, show similar effects on $Q_r$ to the total high clouds (Figure 7). The net warming effect in the atmosphere is robust for all subtypes of high clouds. Since the cirrostratus cloud fraction is larger than the fractions of cirrus and deep convective clouds, cirrostratus makes the largest contribution to the total $Q_r$ than the other two subtypes of high clouds.

### 3.3. High Cloud Fraction Sensitivity to Surface Warming

We define $\Delta C$ and $\Delta T_s$ as the monthly anomaly of cloud fraction and $T_s$, respectively. The short-term sensitivity of cloud fraction to surface warming is obtained as the slope of the linear regression of $\Delta C$ versus $\Delta T_s$ as presented in *Zhou et al*. [2013]. Table 1 shows the slopes of linear regression between $\Delta C$ and $\Delta T_s$ for the averages over the near-global regions, the tropics, and midlatitudes. Student's $t$ tests are carried out for statistical significance. Changes in the total high cloud fraction in response to surface warming vary by region. Total high cloud fraction shows an insignificant decreasing tendency with surface warming in the

**Table 1.** The Slope of Linear Regression Between Area-Averaged High Cloud Fraction Monthly Anomaly and the Global Mean $T_s$ Anomaly During the Period From July 2002 to June 2015 (in Units of % $K^{-1}$)[a]

| | 60°S–60°N | 30°S–30°N | 30°N–60°N | 30°S–60°S |
|---|---|---|---|---|
| Total high cloud | −0.04 ± 0.31 | **−1.00 ± 0.34** | **1.85 ± 0.65** | −0.05 ± 0.64 |
| Cirrus cloud | **0.32 ± 0.11** | 0.01 ± 0.17 | **0.78 ± 0.15** | **0.46 ± 0.16** |
| Cirrostratus cloud | −0.02 ± 0.18 | **−0.64 ± 0.23** | **1.18 ± 0.35** | −0.03 ± 0.38 |
| Deep convection cloud | −0.33 ± 0.18 | **−0.37 ± 0.13** | −0.11 ± 0.30 | −0.48 ± 0.27 |

[a]Bold fonts denote that the regression slope is statistically significant ($p < 0.05$).

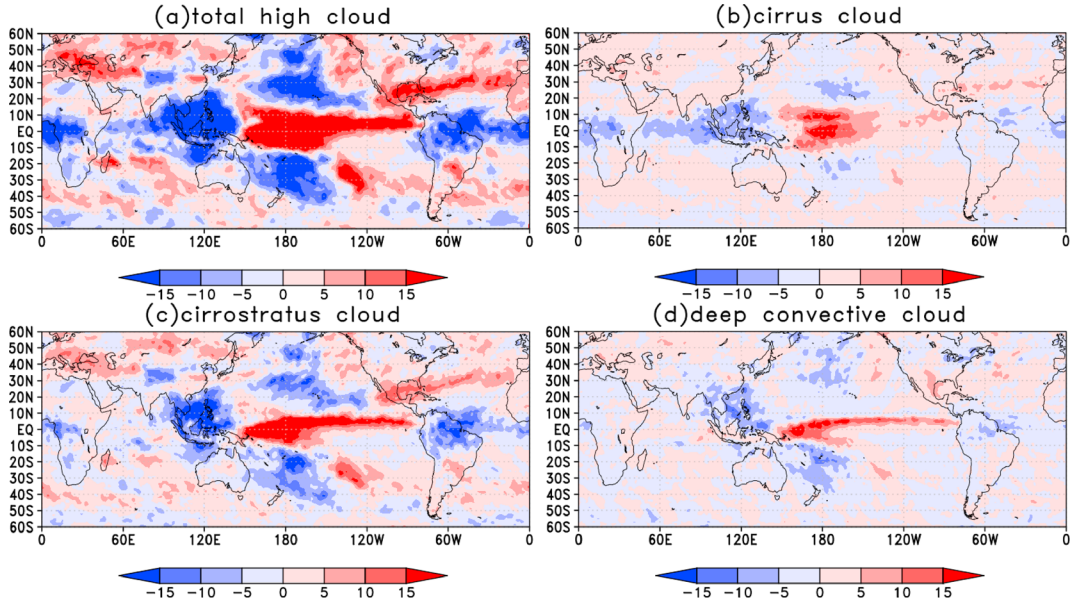


**Figure 8.** The spatial distribution of (a) total, (b) cirrus, (c) cirrostratus, and (d) deep convective cloud fraction sensitivity to the global mean $\Delta T_s$ during the period from July 2002 to June 2015. The units of color bar are % $K^{-1}$.

near-global mean and the southern midlatitudes. However, there is a significant increasing tendency in the northern midlatitudes (1.85 ± 0.65% $K^{-1}$) but a substantial decreasing trend in the tropics (−1 ± 0.3% $K^{-1}$) during the period of 2002–2015. A number of previous studies also reported a reduction in high cloud fraction with increasing $T_s$ in the tropics [e.g., *Lindzen et al*., 2001; *Zelinka and Hartmann*, 2011] but an increase in the northern midlatitudes [e.g., *Wylie and Menzel*, 1999]. Cancelation of cloud fraction sensitivities to surface warming in the northern midlatitudes, southern midlatitudes, and the tropics leads to an insignificant net change in high cloud fraction in the near-global mean.

Regarding different types of high clouds, cirrus clouds display a positive sensitivity to surface warming in four regions, with significant changes in the near-global mean (0.32 ± 0.11% $K^{-1}$) and the midlatitudes, which are consistent with the findings reported in *Zhou et al*. [2014]. Deep convective clouds show a negative sensitivity in four regions, with significant changes in the tropics (−0.37 ± 0.13% $K^{-1}$). Different sensitivities are detected for cirrostratus clouds, for which there is a significant increasing tendency with $T_s$ in the northern midlatitudes and a decreasing tendency in the other three regions. Sensitivities of cirrus and deep convective clouds largely cancel out in the near-global mean and the southern midlatitudes, while the cirrostratus cloud sensitivity in these two regions is slightly negative, leading to an insignificant negative sensitivity of the total high cloud fraction in these two regions. It should be noted that some broken cloud pixels are not included in the MODIS Level 3 joint histograms [*Oreopoulos*, 2005]. However, these broken pixels should not be a serious concern when monthly averaging is performed. For this reason, excluding some broken cloud pixels in the MODIS Level 3 joint histograms may affect to some extent the magnitude of cloud fraction sensitivity to surface warming, rather than the sign.

Figure 8 shows the high cloud fraction sensitivity to surface warming using linear regression $\Delta C$ at each grid box with the global mean $\Delta T_s$ during the period from July 2002 to June 2015, over which temperature changed by about 0.3 K [*NOAA*, 2017]. The spatial distribution of high cloud fraction sensitivities clearly illustrates an El Niño–Southern Oscillation (ENSO)-like pattern, i.e., a characteristic dipole pattern over the tropical Pacific with extensions toward the east at subtropical latitudes along storm tracks [*Su and Jiang*, 2013; *Li et al*., 2017]. The total high cloud fraction depicts a significant positive sensitivity to $T_s$ over actively convective regions such as the Intertropical Convergence Zone. Three subtypes of high clouds show an increase in $\Delta C$ with respect to increasing $\Delta T_s$ over the convective regions in the tropics and decrease over two descending zones of the Hadley cells and the Maritime Continent (MC), representing the impacts of large-scale circulation on high clouds. According to *Kramer and Soden* [2016], the magnitude of hydrological sensitivity in climate model projections differs between interannual variability and long-term trends, suggesting that

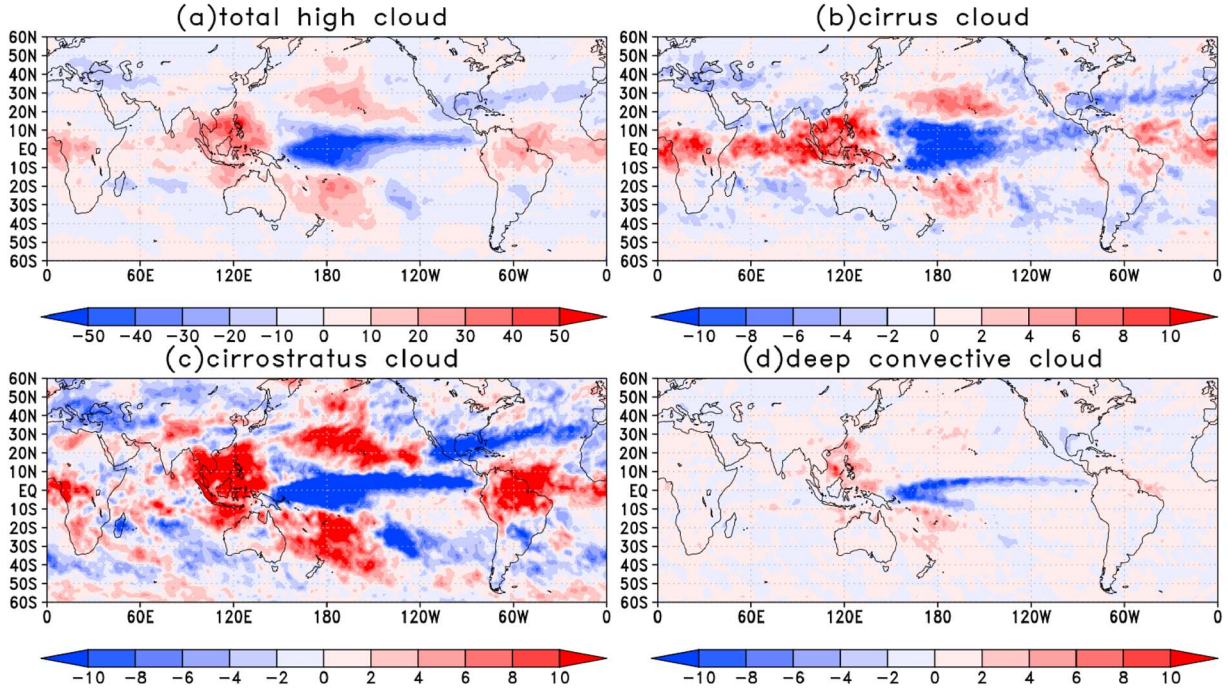


**Figure 9.** The spatial distribution of (a) total, (b) cirrus, (c) cirrostratus, and (d) deep convective clouds CREs on $Q_r$ in response to surface warming (in units of W $m^{-2}$ $K^{-1}$) during the period from July 2002 to June 2015.

cloud radiative feedbacks on $Q_r$ may also vary with timescales. The ENSO-like pattern in Figure 8 suggests that the analysis addresses interannual variability rather than long-term trends. A long-term trend may bear different spatial patterns and magnitude of cloud feedbacks. Thus, one must be cautious when extrapolating interannual variabilities to long-term trends.

### 3.4. Sensitivity of High Cloud Radiative Effect to Increasing Surface Temperature

Taking the sensitivity of high cloud fraction to $T_s$ into consideration, Figure 9 shows the radiative effects on $Q_r$ of the high cloud sensitivity during July 2002 to June 2015. The positive (negative) sensitivity implies that surface warming produces increases (decreases) in $Q_r$, corresponding to a net cooling (warming) effect within the atmosphere.

The spatial distribution of the radiative effects on $Q_r$ of the high cloud sensitivity to $T_s$ resembles the pattern of high cloud fraction sensitivity to surface warming (Figure 8). The most significant ΔCRE occurs over the tropical Pacific. Negative effects on $Q_r$ (i.e., a warming effect within the atmosphere) are observed over central and eastern Pacific, while positive effects are located at two descending zones of the Hadley cells in the Pacific and the MC. Compared with the other two high cloud subtypes, the cirrostratus cloud fraction sensitivity to surface warming is the largest in magnitude over most of the globe, especially over the tropics (Figure 8c); however, because the changes in cirrostratus fraction have both positive and negative signs over a broad area, the average sensitivity of cloud radiative effect of cirrostratus cloud over our analysis domains is not always the largest. For example, the cirrus sensitivity to $T_s$ has the largest radiative effect in the global mean and in the SH midlatitudes (see Table 2).

**Table 2.** Sensitivity of High Cloud Effects on the Atmospheric Cooling Rate During the Period From July 2002 to June 2015 (in Units of W $m^{-2}$ $K^{-1}$)

| | 60°S–60°N | 30°S–30°N | 30°N–60°N | 30°S–60°S |
|---|---|---|---|---|
| Total high cloud | 0.08 | 0.86 | −1.74 | −0.24 |
| Cirrus cloud | −0.27 | −0.04 | −0.69 | −0.49 |
| Cirrostratus cloud | 0.09 | 0.59 | −1.08 | −0.13 |
| Deep convective cloud | 0.03 | 0.04 | −0.03 | 0.12 |

Table 2 shows the effects on $Q_r$ due to high cloud fraction sensitivity to $T_s$ for the near-global region, tropics, and midlatitudes during the study period. The total high cloud fraction sensitivity to $T_s$ would contribute to $Q_r$ at a rate of 0.08 W m$^{-2}$ K$^{-1}$, 0.86 W m$^{-2}$ K$^{-1}$, −1.74 W m$^{-2}$ K$^{-1}$, and −0.24 W m$^{-2}$ K$^{-1}$ for the near-global region, tropics, northern midlatitudes, and southern midlatitudes, respectively. Compared to the cloud-induced $Q_r$ sensitivity to $T_s$ derived from the CERES data that include the effects of all clouds, we find that the FLG-calculated high cloud effects account for 68% of the total cloud effects on $Q_r$ for the global averages.

Based on the FLG calculations, cirrus clouds have a negative effect of −0.27 W m$^{-2}$ K$^{-1}$ and −0.04 W m$^{-2}$ K$^{-1}$ on $Q_r$ in the near-global domain and the tropics, respectively. Cirrostratus clouds have a positive effect of 0.09 W m$^{-2}$ K$^{-1}$ and 0.59 W m$^{-2}$ K$^{-1}$ on $Q_r$ in the near-global domain and the tropics, respectively. Deep convective clouds display a positive effect of 0.03 W m$^{-2}$ K$^{-1}$ in both the near-global case and the tropics. We note that the effects of high cloud fraction sensitivity were computed separately for three subtypes, and the total high cloud effect was not equal to the sum of the effects of three subtypes because of the nonlinearity of radiative calculations.

### 3.5. Contributions of High Cloud Radiative Effects to Precipitation Sensitivity

During the study period from July 2002 to July 2015, $L_vP$ from the GPCP data set increases with $T_s$ at a rate of 4.1 ± 1.1 W m$^{-2}$ K$^{-1}$ and 5.38 W ± 1.48 m$^{-2}$ K$^{-1}$ (4.92 ± 1.36% K$^{-1}$ and 6.1 ± 1.67% K$^{-1}$, relative to multiyear mean precipitation) for the near-global mean and the tropical mean, respectively. The precipitation sensitivity to $T_s$ is dependent on the time period analyzed [*John et al*., 2009]. The global mean sensitivity derived from GPCP and HadCRUT4 temperature is 3.4% K$^{-1}$ for the period of 1989–2010 [*O'Gorman et al*., 2012] and 2.8% K$^{-1}$ for the period of 1988–2010 [*Allan et al*., 2014]. It is clear that large uncertainties still exist in the precipitation sensitivity to $T_s$.

Based on the atmospheric energy constraint on precipitation shown in equation (1), changes in $Q_r$ caused by high cloud response to surface warming would have an impact on the precipitation sensitivity to $T_s$. A positive CRE on $Q_r$ associated with decreases in high cloud fraction would lead to an enhancement in the precipitation sensitivity per unit surface warming. Considering the near-global and the tropical averages, the total high cloud effects on $Q_r$ would account for 1.9 ± 0.7% and 16 ± 6.1% (relative to multiyear mean precipitation) of the precipitation sensitivity to $T_s$, respectively. In terms of three subtypes, we find that cirrus effects reduce precipitation by 6.6 ± 2.5% and 0.72 ± 0.27% for the near-global region and the tropics, respectively, while the responses in cirrostratus to surface warming tend to increase precipitation sensitivity by 2.1 ± 0.8% for the near-global mean and 11.0 ± 4.1% for the tropical mean. Furthermore, the decrease of deep convective cloud fraction with increasing $T_s$ tends to enhance precipitation slightly by 0.81 ± 0.31% for the near-global mean and 0.47 ± 0.18% for the tropical mean during the period of 2002 to 2015.

## 4. Conclusions

In this study, global high clouds including three subtypes (cirrus, cirrostratus, and deep convective cloud) radiative effect on $Q_r$, their sensitivities to surface warming and associated contributions to the precipitation sensitivity per unit surface warming on the interannual timescale during the period from July 2002 to June 2015, have been examined using the FLG plane-parallel radiation model. The FLG calculations are validated against the CERES-EBAF products. The comparison shows that the FLG model captures the temporal variations of all-sky radiative fluxes with reasonable spatial distributions, although large biases exist in the magnitudes of the radiative fluxes and CREs. The FLG model results confirm that the LW warming effect by high clouds outweighs their SW cooling effect in the atmospheric column, leading to a net reduction in $Q_r$ when high clouds increase.

We show that the total high cloud sensitivity to surface warming on the interannual timescale has a positive effect on $Q_r$, due to a decreasing tendency in high cloud fraction in response to surface warming, especially in the tropical mean. In terms of three subtypes of high clouds, cirrostratus and deep convective clouds have a positive effect on $Q_r$, whereas cirrus clouds show a negative effect in the tropics and over the near-global domain.

Furthermore, we find that the interannual precipitation sensitivity per unit surface warming derived from the GPCP data set for the period of 2002 to 2015 is noticeably larger than the prior estimates of 3–4% K$^{-1}$ based

on earlier and longer data record. We suggest that the statistically significant decreasing tendency of tropical mean high cloud fraction with increasing $T_s$ would likely be an important factor in driving the large precipitation sensitivity observed during the A-Train period. Based on our calculations, the decrease of tropical mean high cloud fraction with surface warming would account for about 16 ± 6.1% of the tropical mean precipitation increase per unit surface warming during the period of 2002 to 2015. It is clear that variations of tropical high clouds play a critical role in regulating the sensitivity of precipitation response to interannual surface warming. It should be noted that the time period studied herein is relatively short given the availability of data and that the magnitude of high cloud radiative effects on the hydrological cycle might be related to the timescale considered [*Kramer and Soden*, 2016]. As noted previously, our analysis focuses on the interannual variabilities. Further studies are needed to examine the relation between interannual variations and long-term climate changes of high clouds and precipitation.

**Acknowledgments**
This research was supported by the National Science Foundation under grants AGS-0946315 and AGS-1523296 and the NASA AST and NEWS program. Hui Su and Jonathan Jiang conducted the work at the Jet Propulsion Laboratory, California Institute of Technology, under contract with NASA. We acknowledge the Global Precipitation Analysis, Laboratory for Atmospheres, NASA Goddard Space Flight Center (http://precip.gsfc.nasa.gov/) for providing GPCP data and ECMWF Data Server (http://apps.ecmwf.int/datasets) for providing ERA-Interim reanalysis data. We also acknowledge Clouds and the Earth's Radiant Energy System for providing CERES EBAF-TOA and EBAF-Surface data (available at https://ceres.larc.nasa.gov/order_data.php) and MODerate resolution Imaging Spectroradiometer for providing cloud data (available at ftp://laadsweb.nascom.nasa.gov/NetCDF/L3_Monthly/). Finally, we are grateful to the three anonymous reviewers for their thoughtful comments, which led to an improved revised manuscript.

## References

Adler, R. F., et al. (2003), The version-2 Global Precipitation Climatology Project (GPCP) monthly precipitation analysis (1979–present), *J. Hydrometeorol.*, *4*, 1147–1167, doi:10.1175/1525-7541(2003)004<1147:TVGPCP>2.0.CO;2.

Allan, R. P., C. Liu, M. Zahn, D. A. Lavers, E. Koukouvagias, and A. Bodas-Salcedo (2014), Physically consistent responses of the global atmospheric hydrological cycle in models and observations, *Surv. Geophys.*, *35*, 533–552, doi:10.1007/s10712-012-9213-z.

Allen, M. R., and W. J. Ingram (2002), Constraints on future changes in climate and the hydrological cycle, *Nature*, *419*, 224–232, doi:10.1038/nature01092.

Arking, A. (1991), The radiative effects of clouds and their impact on climate, *Bull. Am. Meteorol. Soc.*, *71*, 795–813, doi:10.1175/1520-0477(1991)072<0795:TREOCA>2.0.CO;2.

Campbell, J. R., S. Lolli, J. R. Lewis, Y. Gu, and E. J. Welton (2016), Daytime cirrus cloud top-of-the-atmospheric radiative forcing properties at a midlatitude site and their global consequences, *J. Applied Meteor. Clim.*, *25*, 1667–1679, doi:10.1175/JAMC-D-15-0217.1.

Dee, D. P., et al. (2011), The ERA-Interim reanalysis: Configuration and performance of the data assimilation system, *Q. J. R. Meteorol. Soc.*, *137*, 553–597, doi:10.1002/qj.828.

European Centre for Medium-Range Weather Forecasts (2002), *The ERA-40 Archive*, p. 40, ECMWF, Reading.

Fu, Q., and K. N. Liou (1992), On the correlated k-distribution method for radiative-transfer in nonhomogeneous atmospheres, *J. Atmos. Sci.*, *49*, 2139–2156, doi:10.1175/1520-0469(1992)049<2139:OTCDMF>2.0.CO;2.

Fu, Q., and K. N. Liou (1993), Parameterization of the radiative properties of cirrus clouds, *J. Atmos. Sci.*, *50*, 2008–2025, doi:10.1175/1520-0469(1993)050<2008:POTRPO>2.0.CO;2.

Fu, Q., K. N. Liou, M. C. Cribb, T. P. Charlock, and A. Grossman (1997), Multiple scattering parameterization in thermal infrared radiative transfer, *J. Atmos. Sci.*, *54*, 2799–2812, doi:10.1175/1520-0469(1997)054<2799:MSPITI>2.0.CO;2.

Gu, Y., J. Farrara, K. N. Liou, and C. R. Mechoso (2003), Parameterization of cloud-radiation processes in the UCLA general circulation model, *J. Clim.*, *16*, 3357–3370, doi:10.1175/15200442(2003)016<3357:POCPIT>2.0.Co;2.

Gu, Y., K. N. Liou, Y. Xue, C. R. Mechoso, W. Li, and Y. Luo (2006), Climatic effects of different aerosol types in China simulated by the UCLA general circulation model, *J. Geophys. Res.*, *111*, D15201, doi:10.1029/2005JD006312.

Gu, Y., K. N. Liou, W. Chen, and H. Liao (2010), Direct climate effect of black carbon in China and its impact on dust storms, *J. Geophys. Res.*, *115*, D00K14, doi:10.1029/2009JD013427.

Gu, Y., K. N. Liou, S. S. Ou, and R. Fovell (2011), Cirrus cloud simulations using WRF with improved radiation parameterization and increased vertical resolution, *J. Geophys. Res.*, *116*, D06119, doi:10.1029/2010JD014574.

Hartmann, D. L., and K. Larson (2002), An important constraint on tropical cloud-climate feedback, *Geophys. Res. Lett.*, *29*(20), 1951, doi:10.1029/2002GL015835.

Hartmann, D. L., and M. L. Michelsen (2002), No evidence for iris, *Bull. Am. Meteorol. Soc.*, *83*, 249–254, doi:10.1175/1520-0477(2002)083>0249:NEFI>2.3.CO;2.

Jiang, J. H., H. Su, C. Zhai, L. Wu, K. Minschwaner, A. M. Molod, and A. M. Tompkins (2015), An assessment of upper-troposphere and lower-stratosphere water vapor in MERRA, MERRA2 and ECMWF reanalyses using Aura MLS observations, *J. Geophys. Res. Atmos.*, *120*, 11,468–11,485, doi:10.1002/2015JD023752.

John, V. O., R. P. Allan, and B. J. Soden (2009), How robust are observed and simulated precipitation responses to tropical ocean warming?, *Geophys. Res. Lett.*, *36*, L14702, doi:10.1029/2009GL038276.

Jones, P. D., and C. Harpham (2013), Estimation of the absolute surface air temperature of the Earth, *J. Geophys. Res. Atmos.*, *118*, 3213–3217, doi:10.1002/jgrd.50359.

Kato, S., N. G. Leob, F. G. Rose, D. R. Doelling, D. A. Rutan, T. E. Caldwell, L. Yu, and R. A. Weller (2013), Surface irradiances consistent with CERES-derived top-of-atmosphere shortwave and longwave irradiances, *J. Clim.*, *26*, 2719–2740, doi:10.1175/jcli-d-12-00436.1.

King, M. D., et al. (2003), Cloud and aerosol properties, precipitable water, and profiles of temperature and water vapor from MODIS, *IEEE Trans. Geosci. Remote Sens.*, *41*, 442–458, doi:10.1109/TGRS.2002.808226.

Kishore, P., M. V. Ratnam, S. P. Namboothiri, I. Velicogna, G. Basha, J. H. Jiang, K. Igarashi, S. V. B. Rao, and V. Sivakumar (2011), Global (50°S–50°N) distribution of water vapor observed by COSMIC GPS RO: Comparison with GPS radiosonde, NCEP, ERA-Interim, and JRA-25 reanalysis data sets, *J. Atmos. Sol. Terr. Phys.*, *73*, 1849–1860, doi:10.1016/j.jastp.2011.04.017.

Kramer, R. J., and B. J. Soden (2016), The sensitivity of the hydrological cycle to internal climate variability versus anthropogenic climate change, *J. Clim.*, *29*, 3661–3673, doi:10.1175/JCLI-D-15-0408.1.

Kuang, Z. M., and D. L. Hartmann (2007), Testing the fixed anvil temperature hypothesis in a cloud-resolving model, *J. Clim.*, *20*, 2051–2057, doi:10.1175/jcli4124.1.

Lambert, F. H., and M. J. Webb (2008), Dependency of global mean precipitation on surface temperature, *Geophys. Res. Lett.*, *35*, L16706, doi:10.1029/2008GL034838.

Lambert, F. H., M. J. Webb, M. Yoshimori, and T. Yokohata (2015), The cloud radiative effect on the atmospheric energy budget and global mean precipitation, *Clim. Dyn.*, *44*, 2301–2325, doi:10.1007/s00382-014-2174-9.

L'Ecuyer, T. S., and J. H. Jiang (2010), Touring the atmosphere aboard the A-Train, *Phys. Today*, *63*, 36–41, doi:10.1063/1.3463626.
Li, K.-F., H. Su, S.-N. Mak, T. M. Chang, and J. H. Jiang (2017), An analysis of high cloud variability: Imprints from the El Niño–Southern Oscillation, *Clim. Dyn.*, *48*, 447–457, doi:10.1007/s00382-016-3086-7.
Lin, B., B. A. Wielicki, L. H. Chambers, Y. Hu, and K. Xu (2002), The iris hypothesis: A negative or positive cloud feedback?, *J. Clim.*, *15*, 3–7, doi:10.1175/1520-0442(2002)015<0003:TIHANO>2.0.CO;2.
Lin, B., T. Wong, B. A. Wielicki, and Y. Hu (2004), Examination of the decadal tropical mean ERBS nonscanner radiation data for the iris hypothesis, *J. Clim.*, *17*, 1239–1246, doi:10.1175/1520-0442(2004)017<1239:EOTDTM>2.0.CO;2.
Lindzen, R. S., and Y.-S. Choi (2011), On the observational determination of climate sensitivity and its implications, *Asia-Pac. J. Atmos. Sci.*, *47*, 377–390, doi:10.1007/s13143-011-0023-x.
Lindzen, R. S., M.-D. Chou, and A. Y. Hou (2001), Does the Earth have an adaptive infrared iris?, *Bull. Am. Meteorol. Soc.*, *82*, 417–432, doi:10.1175/1520-0477(2001)082>0417:DTEHAA>2.3.CO;2.
Liou, K. N., Q. Fu, and T. P. Ackerman (1988), A simple formulation of the delta-four-stream approximation for radiative transfer parameterizations, *J. Atmos. Sci.*, *45*, 1940–1947, doi:10.1175/1520-0469(1988)045<1940:ASFOTD>2.0.CO;2.
Loeb, N. G., B. A. Wielicki, D. R. Doelling, G. L. Smith, D. F. Keyes, S. Kato, N. Manalo-Smith, and T. Wong (2009), Toward optimal closure of the Earth's top-of-atmosphere radiation budget, *J. Clim.*, *22*, 748–766, doi:10.1175/2008JCLI2637.1.
Mace, G. G., Q. Q. Zhang, M. Vaughan, R. Marchand, G. Stephens, C. Trepte, and D. Winker (2009), A description of hydrometeor layer occurrence statistics derived from the first year of merged CloudSat and CALIPSO data, *J. Geophys. Res.*, *114*, D00A26, doi:10.1029/2007JD009755.
Mauritsen, T., and B. Stevens (2015), Missing iris effect as a possible cause of muted hydrological change and high climate sensitivity in models, *Nat. Geosci.*, *8*, 346–351, doi:10.1038/ngeo2414.
Mitchell, J. F. B., C. A. Wilson, and W. M. Cunnington (1987), On $CO_2$ climate sensitivity and model dependence of results, *Q. J. R. Meteorol. Soc.*, *113*, 293–322, doi:10.1002/qj.49711347517.
Morice, G. P., J. J. Kennedy, N. A. Rayner, and P. D. Jones (2012), Quantifying uncertainties in global and regional temperature change using an ensemble of observational estimates: The HadCRUT4 dataset, *J. Geophys. Res.*, *117*, D08101, doi:10.1029/2011JD017187.
NOAA (2017), National Centers for Environmental Information, climate at a glance: Global time series, published December 2016, retrieved on March 1, 2017 from https://www.ncdc.noaa.gov/cag/time-series/global/globe/land_ocean/ytd/12/2002-2015?trend=true&trend_base=10&firsttrendyear=1880&lasttrendyear=2016.
O'Gorman, P. A., R. P. Allan, M. P. Byrne, and M. Previdi (2012), Energetic constraints on precipitation under climate change, *Surv. Geophys.*, *33*, 585–608, doi:10.1007/s10712-011-9159-6.
Oreopoulos, L. (2005), The impact of subsampling on MODIS Level-3 statistics of cloud optical thickness and effective radius, *IEEE Trans. Geosci. Remote Sens.*, *43*, 366–373, doi:10.1109/TGRS.2004.841247.
Pendergrass, A. G., and D. L. Hartmann (2014a), Changes in the distribution of rain frequency and intensity in response to global warming, *J. Clim.*, *27*, 8372–8383, doi:10.1175/JCLI-D-14-00183.1.
Pendergrass, A. G., and D. L. Hartmann (2014b), The atmospheric energy constraint on global-mean precipitation change, *J. Clim.*, *27*, 757–768, doi:10.1175/JCLI-D-13-00163.1.
Rossow, W. B., and R. A. Schiffer (1999), Advances in understanding clouds from ISCCP, *Bull. Am. Meteorol. Soc.*, *80*, 2261–2287, doi:10.1175/1520-0477(1999)080<2261:AIUCFI>2.0.CO;2.
Schröder, M., M. Jonas, R. Lindau, J. Schulz, and K. Fenning (2013), The CM SAF SSM/I-based total column water vapour climate data record: Methods and evaluation against re-analyses and satellite, *Atmos. Meas. Tech.*, *6*, 765–775, doi:10.5194/amt-6-765-2013.
Slingo, A., and J. M. Slingo (1988), The response of a general circulation model to cloud longwave radiative forcing. I: Introduction and initial experiments, *Q. J. R. Meteorol. Soc.*, *117*, 333–364, doi:10.1002/qj.49711448209.
Spencer, R. W., W. D. Braswell, J. R. Christy, and J. Hnilo (2007), Cloud and radiation budget changes associated with tropical intraseasonal oscillations, *Geophys. Res. Lett.*, *34*, L15707, doi:10.1029/2007GL029698.
Stubenrauch, C. J., S. Cros, A. Guignard, and N. Lamquin (2010), A 6-year global cloud climatology from the Atmospheric InfraRed Sounder AIRS and a statistical analysis in synergy with CALIPSO and CloudSat, *Atmos. Chem. Phys.*, *10*, 7197–7214, doi:10.5194/acp-10-7197-2010.
Stubenrauch, C. J., et al. (2013), Assessment of global cloud dataset from satellite: Project and database initiated by the GEWEX radiation panel, *Bull. Am. Meteorol. Soc.*, *94*, 1031–1049, doi:10.1175/BAMS-D-12-00117.1.
Su, H., and J. H. Jiang (2013), Tropical clouds and circulation changes during the 2006–07 and 2009–10 El Niños, *J. Clim.*, *26*, 399–413, doi:10.1175/JCLI-D-12-00152.1.
Su, H., et al. (2008), Variations of tropical upper tropospheric clouds with sea surface temperature and implications for radiative effects, *J. Geophys. Res.*, *113*, D10211, doi:10.1029/2007JD009624.
Su, H., J. H. Jiang, J. D. Neelin, B. H. Kahn, J. W. Waters, N. J. Livesey, and Y. Gu (2010a), Reply to comment by Roberto Rondanelli and Richard S. Lindzen on "Variations in convective precipitation fraction and stratiform area with sea surface temperature", *J. Geophys. Res.*, *115*, D06203, doi:10.1029/2009JD012872.
Su, H., J. H. Jiang, J. D. Neelin, B. H. Kahn, J. W. Waters, N. J. Livesey, and Y. Gu (2010b), Correction to "Reply to comment by Roberto Rondanelli and Richard S. Lindzen on "Observed variations in convective precipitation fraction and stratiform area with sea surface temperature"", *J. Geophys. Res.*, *115*, D06203, doi:10.1029/2010JD014261.
Trenberth, K. E. (2011), Changes in precipitation with climate change, *Clim. Res.*, *47*, 123–138, doi:10.3354/cr00953.
Wang, S., M. Zhang, M. Sun, B. Wang, X. Huang, Q. Wang, and F. Feng (2015), Comparison of surface air temperature derived from NCEP/DOE R2, ERA-Interim, and observations in the arid northwestern China: A consideration of altitude errors, *Theor. Appl. Climatol.*, *119*, 99–111, doi:10.1007/s00704-014-1107-1.
Wielicki, B. A., B. R. Barkstrom, E. F. Harrison, R. B. Lee III, G. L. Smith, and J. E. Cooper (1996), Clouds and the Earth's Radiant Energy System (CERES): An Earth observing system experiment, *Bull. Am. Meteorol. Soc.*, *77*, 853–868, doi:10.1175/1520-0477(1996)077<0853:CATERE>2.0.CO;2.
Wild, M., D. Folini, C. Schär, N. Loeb, E. G. Dutton, and G. König-Langlo (2013), The global energy balance from a surface perspective, *Clim. Dyn.*, *40*, 3107–3134, doi:10.1007/s00382-012-1569-8.
World Meteorological Organization (1975), *International Cloud Atlas Volume I: Manual on the Observation of Clouds and Other Meteors*, vol. 407, p. 180, WMO, Switzerland, Geneva.
Wylie, D. P., and W. P. Menzel (1999), Eight years of high cloud statistics using HIRS, *J. Clim.*, *12*, 170–184, doi:10.1175/1520-0442-12.1.170.
Zelinka, M. D., and D. L. Hartmann (2011), The observed sensitivity of high clouds to mean surface temperature anomalies in the tropics, *J. Geophys. Res.*, *116*, D23103, doi:10.1029/2011JD016459.

Zhang, L., Q. B. Li, Y. Gu, K. N. Liou, and B. Meland (2013), Dust vertical profile impact on global radiative forcing estimation using a coupled chemical-transport-radiative-transfer model, *Atmos. Chem. Phys.*, *13*, 7097–7114, doi:10.5194/acp-13-7097-2013.

Zhao, B., et al. (2016), Impact of buildings on surface solar radiation over urban Beijing, *Atmos. Chem. Phys.*, *16*, 5841–5852, doi:10.5194/acp-16-5841-2016.s.

Zhou, C., M. D. Zelinka, A. E. Dessler, and P. Yang (2013), An analysis of the short-term cloud feedback using MODIS data, *J. Clim.*, *26*, 4803–4815, doi:10.1175/jcli-d-12-00547.1.

Zhou, C., A. E. Dessler, M. D. Zelinka, P. Yang, and T. Wang (2014), Cirrus feedback on interannual climate fluctuations, *Geophys. Res. Lett.*, *41*, 9166–9173, doi:10.1002/2014GL062095.